Applied Catalysis B: Environmental 94 (2010) 125–133

Contents lists available at ScienceDirect

Applied Catalysis B: Environmental

journal homepage: www.elsevier.com/locate/apcatb

Auto-thermal and dry reforming of landfill gas over a $Rh/\gamma Al_2O_3$ monolith catalyst

McKenzie P. Kohn [a], Marco J. Castaldi [a,*], Robert J. Farrauto [a,b]

[a] Earth and Environmental Engineering Department, Columbia University, 500 West 120th Street, New York, NY 10027, USA
[b] BASF Catalysts, 25 Middlesex Turnpike, Iselin, NJ 08830, USA

ARTICLE INFO

Article history:
Received 22 July 2009
Received in revised form 26 October 2009
Accepted 30 October 2009
Available online 10 November 2009

Keywords:
Auto-thermal reforming
Dry reforming
Landfill gas
Rhodium monolith catalyst

ABSTRACT

Auto-thermal and dry reforming of methane and carbon dioxide mixtures was investigated experimentally at temperatures between 300 °C and 800 °C at atmospheric pressures using a $Rh/\gamma Al_2O_3$ monolith catalyst. CH_4:CO_2 ratios of 1:1 and 1.4:1 were tested. The Rh catalyst reached equilibrium conversions of CH_4 and CO_2 to H_2 and CO for both CH_4:CO_2 ratios. Equilibrium analysis shows that carbon formation is likely for dry reforming but not for auto-thermal reforming. Experimentally, carbon formation was seen after long-term exposure to 1.4:1 CH_4:CO_2 ratios without oxygen, but the catalyst has shown the ability to be regenerated in air. Auto-thermal tests, with and without external heat input, operating at an equivalence ratio of 4.3 (O_2:CH_4 = 0.46) and maintaining the CH_4:CO_2 ratio of either 1:1 or 1.4:1, did not show signs of carbon formation or deactivation. ATR experiments resulted in H_2:CO ratios between 1.0 and 2.0 that can be tuned depending on the monolith temperature, beneficial in the case of downstream Fischer–Tropsch processes. For the auto-thermal experiments, theoretical reaction extents were calculated based on experimental data and showed two primary regimes in catalyst operation: a CH_4 combustion and partial oxidation regime, and reforming and water–gas shift regime.

1. Introduction

It is estimated that of the 413 million tons of municipal solid waste (MSW) generated per year in the United States, 64.5% is landfilled [1]. The biomass that makes up 67% of that municipal solid waste anaerobically decomposes in landfills to CH_4 and CO_2. A characteristic landfill gas (LFG) is composed of 45–55% CH_4, 30–40% CO_2, 10–15% N_2, 0–5% O_2, and other trace compounds, but the composition varies depending on the type of waste and the age of the landfill. Approximately 50–100 Nm^3 of methane is generated per ton of MSW landfilled per year, and continues to be generated for at least 50 years after a landfill closes. Currently less than 10% of this is captured and used for energy [2]. This is likely to change as the demand for energy increases making complete and efficient utilization of LFG more important.

As of 2008 there were 565 LFG to energy conversion projects that generate electricity or deliver LFG for direct heating [3] with others being considered to produce liquid natural gas [4]. A challenge of using landfill gas for energy is its low heating value that can result in low flame stability and when combusted can produce more emissions, such as NOx, CO, and unburned hydrocarbons compared to high quality fuels. In addition, the variable composition (CH_4:CO_2 ratios of 1.4:1 to 1:1) makes it difficult to develop a process that yields a consistent output. In these cases, the methane is flared and released as CO_2. One solution to these issues is to catalytically dry reform a portion of the LFG to syngas for more robust combustion. The syngas can also be converted to liquid fuels using Fischer–Tropsch or to a H_2 rich stream using water–gas shift for hydrogen applications.

Dry reforming is a very endothermic reaction and has a high propensity for coke production, especially on base metal catalysts such as Ni [5–7]. Carbon formation on a catalyst can result from either thermodynamically or kinetically governed processes or a combination of both. From a global perspective there are three primary reactions that drive the formation of carbon; CO disproportionation (1), CO reduction (2), and CH_4 decomposition (3) [7]. The dry reforming reaction is also shown below (4). Initially the CH_4 decomposition reaction is kinetically controlled, since there is no H_2 or C in the influent. If carbon is formed during this reaction, as the concentration of carbon increases, the CO disproportionation reverse reaction will initiate to produce CO, which then can react with H_2 to yield C and H_2O via the reduction reaction. The formation of carbon becomes favored as the reaction proceeds due the production of H_2 and CO.

CO disproportionation:

$$2CO \leftrightharpoons CO_2 + C \quad \Delta H = -172\ kJ\ mol^{-1} \tag{1}$$

* Corresponding author.
E-mail address: mc2352@columbia.edu (M.J. Castaldi).

0926-3373/$ – see front matter © 2009 Elsevier B.V. All rights reserved.
doi:10.1016/j.apcatb.2009.10.029

CO reduction:

$$CO + H_2 \leftrightharpoons H_2O + C \quad \Delta H = -131\,kJ\,mol^{-1} \tag{2}$$

CH_4 decomposition:

$$CH_4 \leftrightharpoons 2H_2 + C \quad \Delta H = 75\,kJ\,mol^{-1} \tag{3}$$

Dry reforming:

$$CH_4 + CO_2 \leftrightharpoons 2H_2 + 2CO \quad \Delta H = 247\,kJ\,mol^{-1} \tag{4}$$

Previous studies [5–7,11,12] have shown that dry reforming over a Ni catalyst results in coking that causes the catalyst to quickly deactivate. This is because Ni catalyzes the CO disproportionation, CO reduction, and CH_4 decomposition reactions [7]. Noble metal catalysts such as Rh, however, have not been proven to be as susceptible to carbon formation via these reactions [7,12].

The kinetic mechanisms for dry reforming have been extensively studied for Ni and Rh catalysts. It has been suggested that the mechanism for dry reforming is the stepwise dehydrogenation of methane to surface C, which is then oxidized by co-reactants such as H_2O or CO_2 to form CO and H_2 [5–7,13–15]. The co-reactants may not be kinetically relevant for the dry reforming of CH_4, but they are useful in removing surface carbon and maintaining the activity of the catalyst [14]. The research discussed in this paper investigates the viability of a monolith based Rh/γ-A_2O_3 (stabilized) catalyst to dry reform LFG, and also explores auto-thermal reforming (ATR) as a way to eliminate the need for external heat requirements by generating it internally in a monolithic reactor and reduce the potential for carbon formation.

ATR is the process of introducing small amounts of an oxidant, usually air or O_2, into the fuel stream to convert a portion of the fuel in an exothermic reaction (either combustion or partial oxidation), thereby producing heat in situ necessary for the concurrent endothermic reactions for a net $\Delta H = 0$ kJ mol^{-1}. Several studies have been performed at high space velocities (100 000-400 000 GHSV) and temperatures (up to 1100 °C), elucidating a direct partial oxidation mechanism to produce syngas [16–18] while other studies have been performed at lower space velocities and temperatures (up to 800 °C), resulting in a two step mechanism with combustion and partial oxidation occurring towards the inlet of the catalyst bed and reforming reactions occurring throughout the remainder of the bed [19–20]. This work explores dry and auto-thermal reforming at low space velocities (5000–8000 h^{-1}) and temperatures (up to 700 °C) to better understand the global reactions occurring throughout the catalyst bed.

In the current study it was found that the following global reactions are important in ATR, resulting in more complete conversion of methane to H_2 and CO, and higher H_2:CO ratios compared to dry reforming alone:

Methane combustion

$$CH_4 + 2O_2 \rightarrow 2H_2O + CO_2 \quad \Delta H = -802\,kJ\,mol^{-1} \tag{5}$$

Methane partial oxidation

$$CH_4 + 1/2O_2 \rightarrow 2H_2 + CO \quad \Delta H = -36\,kJ\,mol^{-1} \tag{6}$$

Dry reforming

$$CH_4 + CO_2 \rightarrow 2H_2 + 2CO \quad \Delta H = 247\,kJ\,mol^{-1} \tag{7}$$

Steam reforming

$$CH_4 + H_2O \rightarrow 3H_2 + CO \quad \Delta H = 206\,kJ\,mol^{-1} \tag{8}$$

Water–gas shift

$$H_2O + CO \leftrightharpoons CO_2 + H_2 \quad \Delta H = -42\,kJ\,mol^{-1} \tag{9}$$

The relative importance of these reactions and their contributions is discussed in more detail in Section 3.2.

The majority of studies on methane auto-thermal reforming or partial oxidation have been performed on pellets [18,20,22], foams, or gauzes [16]. This study uses a precious metal wash-coated monoliths because they offer compact reactors with low pressure drop, and have been successfully used in environmental applications since 1975 [8].

2. Experimental methods

Dry and auto-thermal reforming experiments were performed at atmospheric pressure using a quartz flow-through reactor, shown in Fig. 1, and a 4% Rh/γAl_2O_3 wash-coated cordierite monolith (400 cpsi) obtained from BASF Catalysts. The monolith had a bulk density of 0.44 g cm^{-3} and washcoat loading of 1.2 g cm^{-3}. The quartz-reactor assembly was placed in a two-stage furnace (Applied Test Systems, Inc, 3210 Series) controlled with Omega temperature controllers (CN9000A Series). One thermocouple (Omega K-type, KMQIN-020U) was inserted 1/16″ into a channel of the monolith at the exit to measure the monolith outlet temperature. In some experiments, a thermocouple (Omega K-type, KMQIN-020U) was also inserted 1/16″ into a channel at the entrance of the monolith to measure the monolith inlet temperature. Temperature readings were acquired with a continuous data acquisition system (Omega, OMB-DAQ-55). The mass flow rate of reactant gases into the reactor were controlled with Aalborg mass flow controllers (GFC17) that were supplied from gas cylinders of UHP CH_4, CO_2, N_2 and Zero grade O_2 (TechAir). The reactor was coupled to an on-line Agilent Micro GC (QUAD)

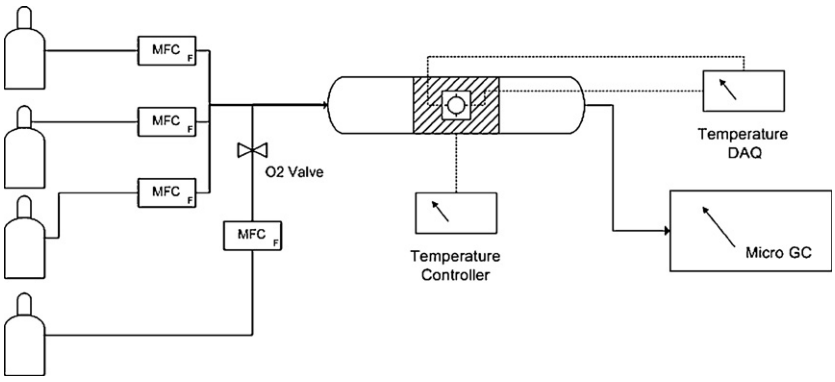

Fig. 1. Schematic of apparatus.

instrument to measure the gas product composition. Chemical equilibrium concentrations were calculated with GASEQ [9] for gaseous product species and with HSC 5.11 [10] for solid carbon species.

One way to determine the amount of oxygen needed for a theoretical net enthalpy of zero is to assume that primarily complete methane combustion and dry reforming would occur. Therefore, each mole of methane will react with 0.46 mol of O_2, shown in the following global reaction.

$$1.0CH_4 + 0.77CO_2 + 0.46O_2 \rightarrow$$
$$1.54CO + 1.54H_2 + 0.23CO_2 + 0.46H_2O \quad \Delta H = 0\,\text{kJ mol}^{-1} \quad (10)$$

A common way to express the amount of oxidant required to balance the enthalpy is to use an equivalence ratio Φ, defined below.

$$\Phi = \frac{A/F_{\text{stoichiometric}}}{A/F_{\text{actual}}}$$

where A represents air or oxygen and F represents fuel, methane only in this case. Therefore all of the ATR experiments discussed in this paper used a reactant input stream with approximately a 0.46 O_2 to CH_4 ratio, or $\Phi = 4.3$.

Landfill gas can vary in composition from a 1:1 to 1.4:1 CH_4:CO_2 ratio depending on several factors. To ensure a complete understanding of reforming landfill gas, both of these extremes were tested. Initially 1:1 CH_4:CO_2 mixtures in approximately 80% N_2 were studied. This resulted in an initial data set and provided guidance for subsequent experiments. More representative LFG mixtures were then tested that were comprised of 1.4:1 CH_4:CO_2 mixtures in 13.5% N_2. For each case, both dry reforming and ATR conditions were investigated. For the auto-thermal tests, oxygen was added to yield a target equivalence ratio of 4.3, maintaining the CH_4:CO_2 ratio of either 1:1 or 1.4:1, depending on the experiment type. The resulting mole fractions of these product streams are shown in Table 1.

3. Results and discussion

3.1. Carbon formation regime calculation

To better understand the operating regimes where thermodynamic carbon formation is favored, several steady state thermodynamic calculations were performed using HSC 5.11 and GASEQ for a range of O:C and H:C ratios at atmospheric pressure. Equilibrium calculations from 25 °C to 1200 °C for CH_4:CO_2 ratios of 1:1 predicted the most amorphous carbon at approximately 450 °C. Equilibrium calculations for CH_4:CO_2 ratios of 1.5:1 predicted solid carbon at approximately 450 °C, and in the range 800–1200 °C in which CO_2 is depleted but CH_4 is still present. Because the temperature range investigated in the majority of the experiments presented here is from 300 °C to 700 °C, the thermodynamic carbon formation at 450 °C as a function of O:C, H:C, O_2:CH_4, and CO_2:CH_4 ratios is represented as the shaded area in Fig. 2. Fig. 2 shows that carbon formation is most favored at low O_2:CH_4 ratios and high CO_2:CH_4 ratios.

Table 1
Resulting mole fraction of reactant gases for each experiment type.

	CH_4:CO_2 = 1:1		CH_4:CO_2 = 1.4:1	
CH_4 (%)	8.3	8.0	51.0	41.0
CO_2 (%)	8.3	8.0	35.5	29.0
N_2 (%)	83.4	80.3	13.5	11.0
O_2 (%)	0	3.7	0	19.0
Φ	0.0	4.3	0.0	4.3

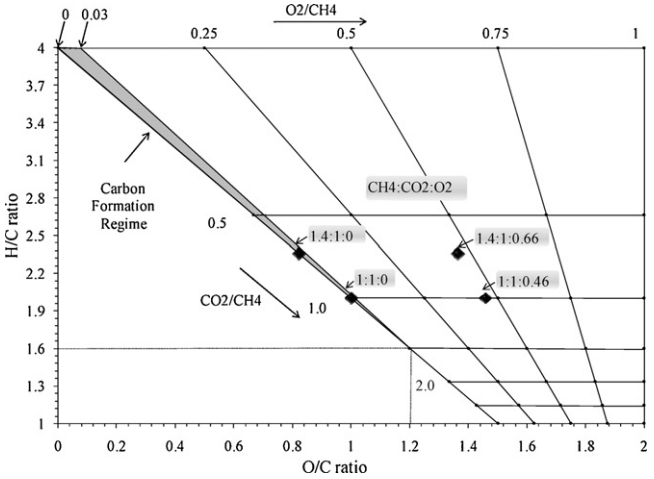

Fig. 2. Thermodynamic carbon formation regime at 450 °C and 1 atm.

Both the thermodynamic and kinetic mechanisms for dry reforming result in surface carbon that must be removed using oxygenated species either in the catalyst support or in the gas feed to maintain the activity of the catalyst. O_2 has a higher oxidation potential than CO_2 or H_2O, so it is ideal for removing surface carbon. This is shown in Fig. 2, where at least 1.5 mol of CO_2 is needed per mole of CH_4 to be outside of the carbon formation regime, but only 0.03 mol of O_2 is needed per mole of CH_4. One motivation for auto-thermally reforming CH_4 is that the addition of an oxidant reduces the likelihood of carbon formation. To obtain an understanding of dry and auto-thermally reforming LFG mixtures, this work focused on two points in the dry reforming regime, shown in Fig. 2 corresponding to CH_4:CO_2:O_2 ratios of 1.4:1:0 and 1:1:0, and two points in the ATR regime, corresponding to CH_4:CO_2:O_2 ratios of 1.4:1:0.66 and 1:1:0.46.

3.2. Dry reforming vs. auto-thermal reforming for 1:1 CH_4:CO_2 mixtures in 83% N_2

A large body of literature exists on the mechanisms of dry reforming with various catalysts and operating conditions [5–7,11,13,23–26]. This section will focus on the differences between dry reforming and auto-thermal reforming for 1:1 CH_4:CO_2 mixtures in 83.4% N_2. The insights gained here will then be extended to CH_4:CO_2 ratios of 1.4:1 in 13.5% N_2 that are more characteristic of an actual landfill gas.

Because CH_4 dry reforming at a CH_4:CO_2 ratio of 1:1 or greater is susceptible to carbon formation according to the carbon formation regime shown in Fig. 2, a set of tests were conducted with high dilution to minimize carbon deposition. Fig. 3 shows chemical species concentration as a function of reactor temperature for a mixture with a CH_4:CO_2 ratio of 1:1 in 83.4% N_2 at 5000 h^{-1} GHSV. Also shown in Fig. 3 are the results of a chemical equilibrium calculation to provide a basis for comparison. As the gas temperature increases, the CH_4 and CO_2 are more fully converted to CO and H_2. Throughout this experiment, no visible coking or catalyst deactivation was seen. H_2O is produced in the dry reforming reaction, shown in Fig. 3, due to the reverse water–gas shift reaction. This is why the CO_2 concentration drops below the CH_4 concentration at 420 °C, although the dry reforming reaction stoichiometry dictates that CH_4 and CO_2 would be consumed at a 1:1 ratio. This change in CO_2 is reflected in the data. Overall the data follows closely to the equilibrium values. At low temperatures, between 350 °C and 450 °C, the data is approximately 40% away from the equilibrium calculations. The difference can be explained by the lag in temperature between the inlet gas and the

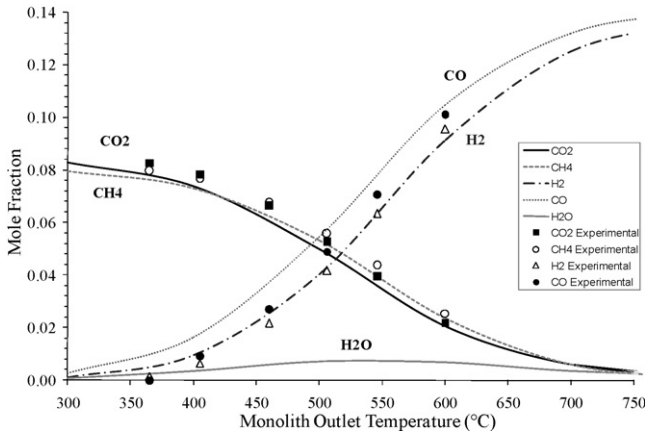

Fig. 3. Dry reforming of a 1:1 CH_4:CO_2 mixture in 83% N_2 with Rh catalyst at 8000 h^{-1} GHSV.

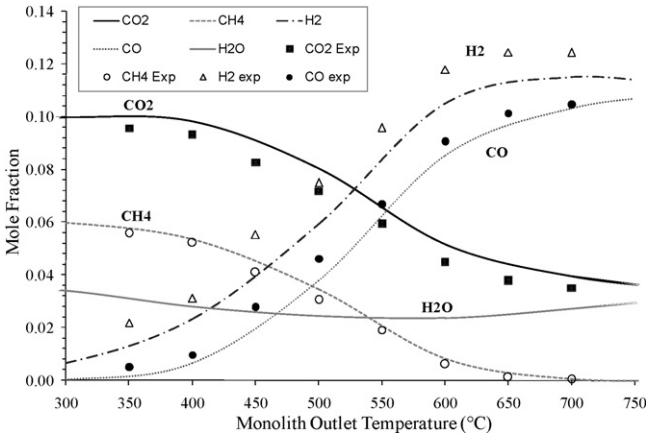

Fig. 4. Auto-thermal reforming of a 1:1 CH_4:CO_2 mixture in 80% N_2 with Rh catalyst at 8000 h^{-1} GHSV.

monolith surface, which is not surprising since the dry reforming reaction is endothermic. The difference between data and the equilibrium calculation becomes smaller as temperature increases, for example at 600 °C, H_2 is 1.5% above equilibrium and CO is 6.0% below equilibrium.

To obtain an understanding of the primary differences between dry reforming and ATR, an experiment was performed with identical CH_4 and CO_2 ratios, with 3.6% O_2 added with N_2 balance. This resulted in a CH_4:CO_2:O_2 ratio of 1:1:0.46 at 8000 h^{-1} GHSV. Figs. 4 and 5 show the results of this experiment for chemical species concentration as a function of monolith outlet temperature. Fig. 4 also shows the results of a chemical equilibrium calculation to compare to experimental data, while Fig. 5 shows temperatures from 0 °C to 300 °C to capture the catalyst light off. Fig. 4 shows that larger amounts of H_2O and CO_2 are predicted due to the combustion of CH_4 and O_2, compared to the dry reforming experiment shown in Fig. 3. In general, the species concentrations follow equilibrium, particularly CH_4. However, at 600 °C, CO_2 is

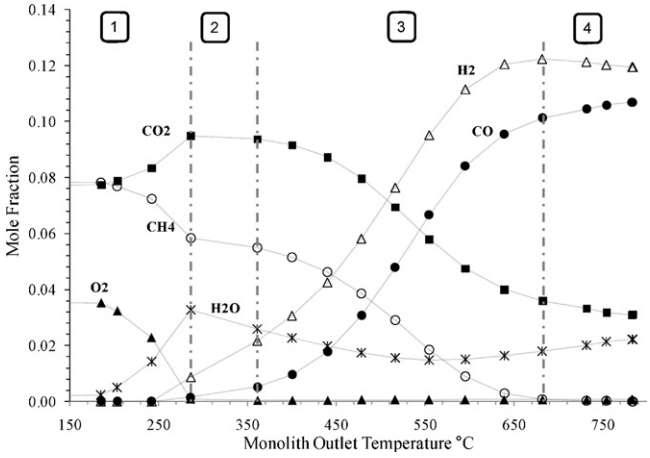

Fig. 5. ATR reaction regions for CH_4:CO_2:O_2 ratio of 1:1:0.46 in 80% N_2 at 8000 h^{-1} GHSV on Rh catalyst.

10% lower than predicted by equilibrium, and H_2 and CO are 10% and 2% higher than equilibrium, respectively. This discrepancy may be due to higher extents of partial oxidation, as opposed to methane combustion, than what is predicted by equilibrium. As expected from these reaction conditions which are located outside of the carbon formation regime shown in Fig. 2, no noticeable coking or deactivation was seen during this experiment.

In Fig. 5, two heating rates are shown: roughly before and after catalytic CH_4 ignition, which occurred between 200 °C and 286 °C. For the first heating rate the monolith was heated from 24 °C to 286 °C at a rate of 220 °C h^{-1}. For the second rate, after CH_4 ignition, the monolith was heated from 286 °C to 800 °C at 150 °C h^{-1}. Table 2 shows the product mole fraction at selected points throughout the experiment to provide a quantitative comparison. All of the mole fractions are measured, except for H_2O, which was calculated based on a H_2 balance. The data is divided into four reaction regions based on the likely dominant reactions.

In Fig. 5, starting from the left at a temperature of 150 °C, we observe that CH_4 combustion begins at approximately 203 °C, reaching a maximum at 286 °C, where oxygen is rapidly consumed with a commensurate consumption of 2.1% CH_4, from 7.9% to 5.8%, and a production of 1.8% CO_2, from 7.7% to 9.5% and 3.2% H_2O, from 0.1% to 3.3%, as shown in Table 2. These measured mole fractions coincide well with the stoichiometry of the combustion reaction $CH_4 + 2O_2 \rightarrow 2H_2O + CO_2$. This suggests that combustion is the dominant reaction in this region. However, 0.9% H_2 and 0.1% CO are also produced, suggesting that partial oxidation or water-gas shift may also occur to some extent in this region.

In region 2, as the monolith exit temperature is increased from 286 °C to 361 °C, 0.3% CH_4 (5.8–5.5%), 0.7% H_2O (3.3–2.6%), and 0.1% CO_2 (9.5–9.4%) are consumed. Also in this region, 1.2% H_2 (0.9–2.1%) and 0.4% CO (0.1–0.5%) are produced, resulting in a H_2:CO ratio of 4.2 The relatively high consumption of water and resulting H_2:CO ratio of 4.2 indicate that steam reforming ($CH_4 + H_2O \rightarrow 3H_2 + CO$) may be the dominant reaction in this

Table 2
Product distribution at selected temperatures during experiment with CH_4:CO_2:O_2 ratio of 1:1:0.46 in 80% N_2 at 8000 h^{-1} GHSV on Rh catalyst.

Monolith outlet temperature (°C)	CO_2	CH_4	H_2	CO	O_2	H_2O	H_2/CO ratio
150	7.7%	7.9%	0.0%	0.0%	3.6%	0.1%	0.0
286	9.5%	5.8%	0.9%	0.1%	0.1%	3.3%	9.0
361	9.4%	5.5%	2.1%	0.5%	0.0%	2.6%	4.2
516	6.9%	2.9%	7.6%	4.8%	0.1%	1.6%	1.6
682	3.6%	0.1%	12.2%	10.1%	0.1%	1.8%	1.2
783	3.1%	0.0%	11.9%	10.7%	0.1%	2.2%	1.1

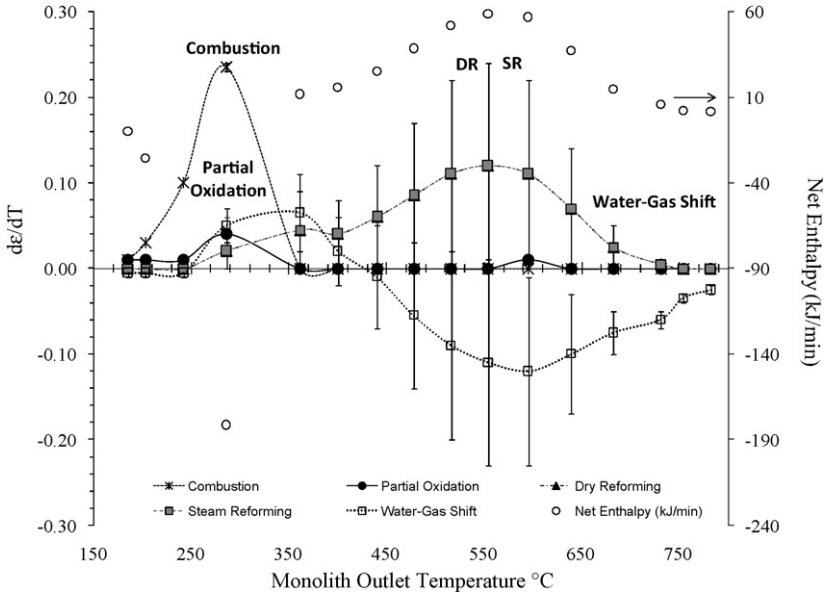

Fig. 6. Extent of reactions occurring for CH_4:CO_2:O_2 ratio of 1:1:0.46 at 8000 h^{-1} GHSV on a Rh catalyst as a function of monolith outlet temperature.

region, along with some extent of dry reforming and water–gas shift.

As the monolith exit temperature is further increased from 361 °C to 682 °C in region 3, the H_2:CO ratio decreases from 4.2% to 1.2. 5.8% CO_2 (9.4–3.6%), 5.4% CH_4 (5.5–0.1%), and 0.8% H_2O (2.6–1.8%) are consumed while 10.1% H_2 (2.1–12.2%) and 9.6% CO (0.5–10.1%) are produced. Because approximately equal amounts of CO_2 and CH_4 are consumed, and the resulting H_2:CO ratio is 1.2, dry reforming ($CH_4 + CO_2 \rightarrow 2H_2 + 2CO$) may be the dominant reaction in this region.

In region 4, as the monolith exit temperature is increased from 682 °C to 783 °C, H_2:CO ratio continues to decrease from 1.2 to 1.1. In this region there is little CH_4 left to react; CH_4 concentration decreases from 0.1% to 0%. 0.5% CO_2 (3.6–3.1%) and 0.3% H_2 (12.2–11.9%) are consumed while 0.4% H_2O (1.8–2.2%) and 0.6% CO (10.1–10.7%) are produced. These mole fractions coincide well with the reverse water–gas shift reaction; $CO_2 + H_2 \rightarrow H_2O + CO$.

Further insight into the occurrence and sequence of these reactions can be obtained from a reaction extent calculation that helps quantify the extent of reactions that are occurring throughout the auto-thermal reforming experiment shown in Fig. 5. The calculation assumes that the following five global reactions may occur to any extent, denoted by ε, at any temperature to give the molar fractions, denoted by χ, of the product species: CH_4, CO_2, H_2, CO, H_2O, and O_2.

$$\left.\begin{array}{l} CH_4 + 2O_2 \rightarrow 2H_2O + CO_2 \;\varepsilon_{Comb} \\ CH_4 + \frac{1}{2}O_2 \rightarrow 2H_2 + CO \;\varepsilon_{POX} \\ CH_4 + H_2O \rightarrow 3H_2 + CO \;\varepsilon_{SR} \\ CH_4 + CO_2 \rightarrow 2H_2 + 2CO \;\varepsilon_{DR} \\ H_2O + CO \rightarrow CO_2 + H_2 \;\varepsilon_{WGS} \end{array}\right\} = \chi_{CH_4}, \chi_{CO_2}, \chi_{H_2}, \chi_{CO}, \chi_{H_2O}, \chi_{O_2}$$

For many temperature increments of approximately 40 °C, the change in reaction extents over each temperature interval that produced theoretical product concentrations within 6% of the experimental mole fractions in Fig. 5 were found. In many cases there was not a unique solution, therefore median values were plotted and error bars represent the range of reaction extents that could occur to produce molar flow rates no further than 6% from those found experimentally.

The calculation results are shown in Fig. 6, which displays the $d\varepsilon/dT$ (left ordinate) and the net enthalpy of reaction (right ordinate) vs. monolith outlet temperature. At a monolith temperature of 286 °C, it is clear that combustion is the dominant reaction, and partial oxidation is occurring to a lesser extent. Above 440 °C, dry reforming and steam reforming lines overlap, and reverse water–gas shift may be occurring, but the error bars are very large. This is due to the fact that the sum of steam reforming and water–gas shift is stoichiometrically equal to dry reforming, and therefore dry reforming and steam reforming are indistinguishable when water–gas shift is occurring using this stoichiometric calculation method. The plot does show the transition region between the combustion and partial oxidation reactions and the reforming reactions that occurs at approximately 360 °C. This plot shows that there are primarily two regimes: a combustion/partial oxidation regime and a reforming/water–gas shift regime, confirming previously reported literature [18–21]. The reforming/water–gas shift regime is in agreement with previous reports that steam and dry reforming occur with the water-gas shift reaction [15]. However, knowledge of the relative kinetics of the reforming and water–gas shift reactions would be necessary to differentiate the extents of those reactions, making further investigation warranted.

The net enthalpy shown on the right ordinate was calculated based on experimental molar flow rates of the product species. The enthalpy calculation shows that early in the reaction, at a monolith outlet temperature of 286 °C, where the exothermic combustion and partial oxidation reactions are occurring, the net enthalpy of reaction is negative. As the monolith temperature increases and reforming occurs, the net enthalpy increases to zero. These calculations predict that under these reaction conditions and inlet CH_4:CO_2 ratio, assuming the reactor is adiabatic, auto-thermal operation could be achieved between a monolith outlet temperature of 640 °C and 680 °C. Auto-thermal operation was achieved in this research and will be discussed in Section 3.4.

3.3. Dry reforming vs. auto-thermal reforming for 1.4:1 CH_4:CO_2 mixtures

An understanding of dry and auto-thermal reforming CH_4:CO_2 ratios of 1:1 in 83% N_2 provided insight on reforming CH_4:CO_2 ratios of 1.4:1 composed of approximately 51% CH_4, 35% CO_2, and

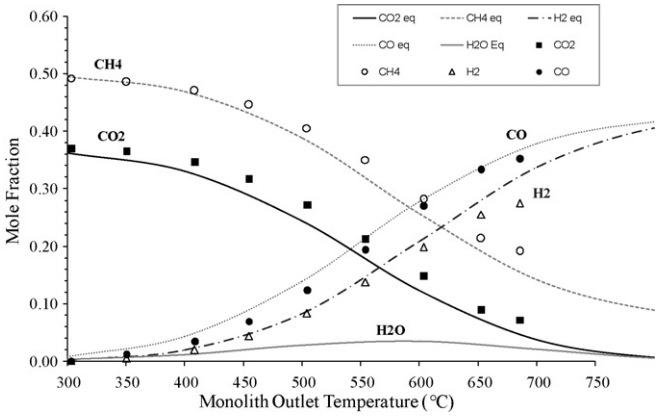

Fig. 7. Dry reforming a mixture with CH_4:CO_2 ratio of 1.4:1 in14% N_2 at 5000 h^{-1} GHSV on Rh catalyst.

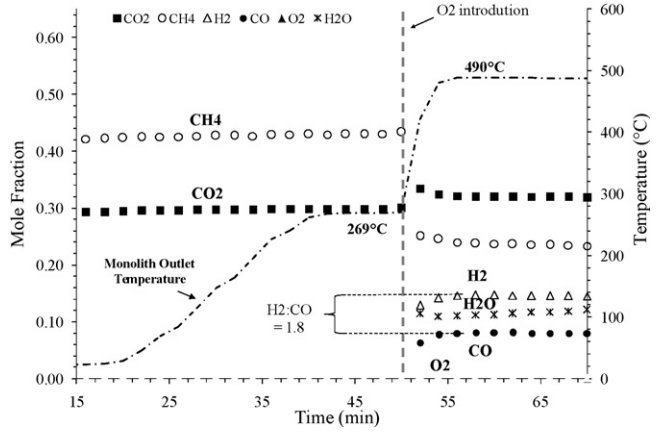

Fig. 8. Effect of 19% O_2 introduction at 269 °C into a CH_4:CO_2 ratio of 1.4:1 in 13% N_2 at 8000 h^{-1}.

13.5% N_2; compositions characteristic of an actual LFG. Fig. 7 shows chemical species concentration as a function of monolith outlet temperature for this mixture with a CH_4:CO_2 ratio of 1.4:1 with 13.5% N_2 at 5000 h^{-1} GHSV. The result of a chemical equilibrium calculation is also shown. As the reactor temperature increases, the CH_4 and CO_2 are more fully converted to CO and H_2, closely following equilibrium predictions. After aging in this gas mixture for 24 h at 700 °C some carbon formation occurred as evidenced by a loss of catalyst activity and darkening of the monolith. However, other experiments not discussed in detail here have shown that after coking, the Rh catalyst can be regenerated in air, resulting in an evolution of CO_2 and activity recovery.

Again, to understand the differences between dry reforming and ATR, and how O_2 introduction can be used to reform landfill gases with CH_4:CO_2 ratios of approximately 1.4:1, a series of experiments were performed with a CH_4:CO_2 ratio of 1.4:1, with 19% O_2 added. The resulting mixture was approximately 41% CH_4, 29% CO_2, 11% N_2 and 19% O_2 and the resulting mole ratio was CH_4:CO_2:O_2 = 1.4:1:0.66, or Φ = 4.3, at 8000 h^{-1} GHSV. In each experiment, CH_4, CO_2, and N_2 were introduced into the reactor without O_2 present. The monolith was heated to a particular temperature and allowed to stabilize, and then O_2 was introduced. This was performed for monolith outlet temperatures of 269 °C, 361 °C, 443 °C, and 513 °C.

Fig. 8 shows the results of this type of experiment with O_2 introduced at a monolith temperature of 269 °C. Mole fraction is shown on the left ordinate and monolith outlet temperature is shown on the right ordinate. The dashed grey vertical line shows the time at which the O_2 is introduced. Before O_2 introduction, CH_4 and CO_2 concentrations are stable while the monolith is heated to 269 °C. After O_2 introduction, there is a sharp rise in the monolith outlet temperature, and CO_2, H_2, H_2O, and CO are produced, while CH_4 is consumed. The O_2 is consumed so rapidly that only a slight amount of O_2 is visible in the data. The sharp increase in monolith outlet temperature, up to 490 °C, consumption of CH_4, and production of CO_2 and H_2O indicate that methane combustion occurs rapidly. The simultaneous production of H_2 and CO at a H_2:CO ratio of 2.0 indicates that partial oxidation, steam reforming, dry reforming, or water–gas shift may also be occurring. The reactor was then heated until the monolith reached an outlet temperature of approximately 550 °C, so that it could be compared to other experiments, as shown in Tables 3 and 4. Table 3 shows the mole fractions of H_2 and CO as a function of monolith temperature and O_2 introduction temperature for reforming CH_4:CO_2 mixtures of 1.4:1 with 11% N_2 and, in the ATR cases, 19% O_2. Table 4 shows CH_4 conversion as a function of monolith temperature and O_2 introduction temperature for the same reaction conditions.

Fig. 9 shows the results of the exact same experiment, except that O_2 is introduced at 443 °C. In this case the CH_4 and CO_2 begin to react at 300 °C before O_2 introduction. At 443 °C, before O_2 introduction, 5% of the methane is consumed most likely via dry reforming to form H_2 and CO at a H_2:CO ratio of 0.66. After O_2 introduction at 443 °C (Fig. 9), the monolith outlet temperature increases to 554 °C, resulting in a H_2:CO ratio of 1.27. The reactor was then heated until the monolith reached an outlet temperature of approximately 600 °C, so that it could be compared to other experiments, as shown in Tables 3 and 4. These experiments were repeated for O_2 introduction temperatures of 361 °C and 513 °C. The results of these experiments are also shown in Tables 3 and 4.

Figs. 8 and 9 show the monolith outlet temperature as a result of O_2 introduction and as a function of the furnace temperature. Typically, the exothermic methane combustion reaction occurs rapidly at the inlet of the monolith, and the endothermic reforming reactions occur throughout the remainder of the monolith, resulting in higher temperature at the inlet of the monolith compared to the downstream end of the monolith [16–20]. Therefore, the monolith outlet temperature is a reflection of all exothermic and endothermic reactions occurring throughout the

Table 3
ATR results in greater production of H_2 and CO for CH_4:CO_2 ratios of 1.4:1 in 13.5% N_2 at 8000 h^{-1} GHSV on a Rh catalyst.

Monolith outlet temperature (°C)	O_2 @ 269 °C		O_2 @ 361 °C		O_2 @ 443 °C		O_2 @ 513 °C		Dry reforming	
	H_2	CO	H_2	CO	H_2	CO	H_2	CO	H_2	CO
250	0%	0%	0%	0%	0%	0%	0%	0%	0%	0%
300			0%	0%	0%	0%	0%	0%	0%	0%
350			1%	2%	0%	1%	0%	1%	0%	1%
400	13%	6%			2%	3%	1%	2%	2%	3%
450	14%	8%			4%	6%	5%	7%	4%	7%
500	16%	9%	19%	12%			8%	14%	8%	12%
550	20%	13%	24%	17%	22%	17%			13%	19%
600			32%	26%	27%	21%	28%	22%	19%	26%

Table 4
CH_4 conversion for CH_4:CO_2 ratios of 1.4:1 in 13.5% N_2 at 8000 h^{-1} GHSV on a Rh catalyst.

Monolith outlet temperature (°C)	O_2 @ 269 °C	O_2 @ 361 °C	O_2 @ 443 °C	O_2 @ 513 °C	Dry reforming
250	0%	0%	0%	0%	0%
300		0%	0%	1%	0%
350		0%	2%	1%	1%
400	33%		4%	3%	3%
450	34%		5%	7%	6%
500	39%	37%		13%	11%
550	47%	50%	48%		18%
600		63%	63%	63%	29%

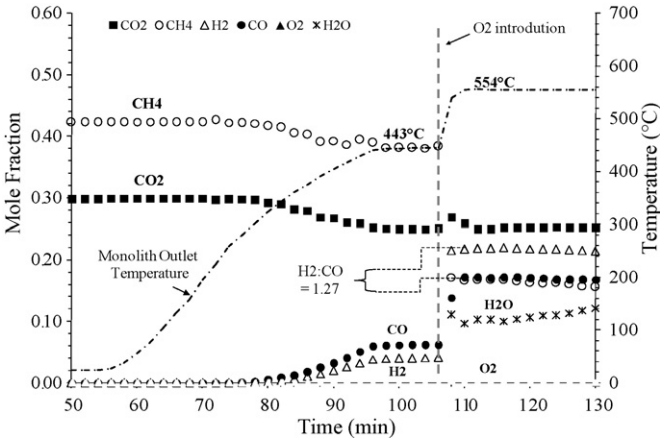

Fig. 9. Effect of 19% O_2 introduction at 443 °C into a CH_4:CO_2 ratio of 1.4:1 in 13% N_2 at 8000 h^{-1} GHSV on a Rh catalyst.

monolith. This temperature gradient is discussed further in Section 3.4, where the difference between the monolith inlet and outlet temperature is shown in Fig. 11.

In each O_2 introduction experiment, after O_2 introduction, the product concentrations were within 6% of expected equilibrium values. Furthermore, after O_2 introduction, the concentrations of products and methane conversion were nearly identical at the same monolith outlet temperatures, as shown in Tables 3 and 4. Another example of this is shown in Fig. 10, which shows the various H_2:CO ratios that can be achieved as a function of the monolith outlet temperature. H_2:CO ratios achieved by dry reforming are shown to compare to the auto-thermal reforming cases. The H_2:CO ratios produced from dry reforming increase from approximately 0.38 at 350 °C to 0.77 at 650 °C, and the ratios

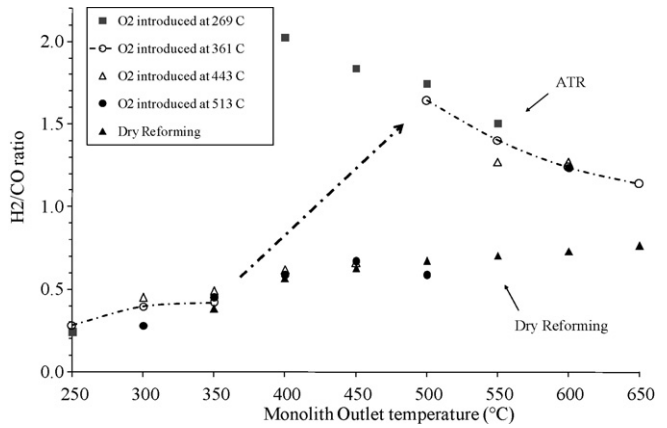

Fig. 10. Effect of O2 introduction and monolith outlet temperature on H_2:CO ratio for CH_4:CO_2 ratios of 1.4:1 in 13% N_2 at 8000 h^{-1} GHSV on a Rh catalyst.

produced from auto-thermal reforming decrease from 2.02 at 400 °C to 1.14 at 650 °C. Before O_2 introduction, experimental data lays on the dry reforming line, while after O_2 introduction, the data lays on the same ATR line. This is illustrated for the O_2 introduction at 361 °C case by the dotted line. Before 361 °C, the H_2:CO ratios increased from 0.28 at 250 °C to 0.45 at 350 °C, following the dry reforming line. After O_2 was introduced, the H_2:CO ratio increased to 1.64 at a temperature of 500 °C and then decreased to 1.14 at 650 °C, falling on the auto-thermal reforming line.

In both Table 3 and Fig. 10, the difference in H_2:CO ratios between dry reforming and auto-thermal reforming is the greatest at low monolith outlet temperatures most likely due to the occurrence of partial oxidation producing syngas directly, as shown in Fig. 6. As the monolith outlet temperature increases above 450 °C, into the reforming regime, the H_2:CO ratios decreases as shown in Fig. 10. Above 650 °C, reverse water–gas shift may occur, further lowering the H_2:CO ratio. As the monolith is heated, the H_2:CO ratios produced from dry reforming and ATR converge to one, the ratio predicted from the stoichiometry of the dry reforming reaction. These experiments therefore show that equilibrium is achieved after introducing O_2 into the reactor, and that the H_2:CO ratio can be adjusted by varying the monolith, or reactor temperature.

Although the combustion of CH_4 may not be advantageous in some instances, in LFG mixtures with CH_4:CO_2 ratios of higher than 1:1, the combustion is very useful. In these cases, without O_2 introduction, the excess CH_4 would remain unreacted due to sub-stoichiometric amounts of CO_2. With ATR, some of this excess CH_4 can be combusted to produce heat in the monolith that enhances the rate of the reforming reactions. In addition, CO_2 and H_2O are produced from the methane combustion, which react with the remaining CH_4 to ensure that all of the CH_4 can be converted to syngas at higher H_2:CO ratios than dry reforming alone.

Tables 3 and 4 show that although some CH_4 is combusted in ATR, the heat and reactants provided by the combustion result in greater syngas production compared to dry reforming. As the monolith temperature increases, in both ATR and dry reforming the total mole fraction of H_2 and CO increases. However, ATR produces more syngas because of the heat and reactants supplied by the combustion of excess CH_4, and because some partial oxidation occurs, producing more H_2 and CO. It is important to note here that the concentrations presented in Table 3 assume that oxygen is supplied using pure O_2 for auto-thermal reforming; only 11% N_2 is added to the feed to simulate a characteristic landfill gas. If air is used for ATR instead of pure oxygen, the product concentrations will be diluted in 80% N_2.

Auto-thermal reforming produces heat in the channels of the monolith, leading to higher conversion of CH_4 to syngas. This lowers the required heat input for the reforming processes, or, in auto-thermal operation, eliminates the need for constant heat input. The combustion reaction also produces H_2O and CO_2 that react with the remaining CH_4 to form H_2 and CO. ATR produces a range of H_2:CO ratios from 1.0 to 2.0, as a function of the monolith

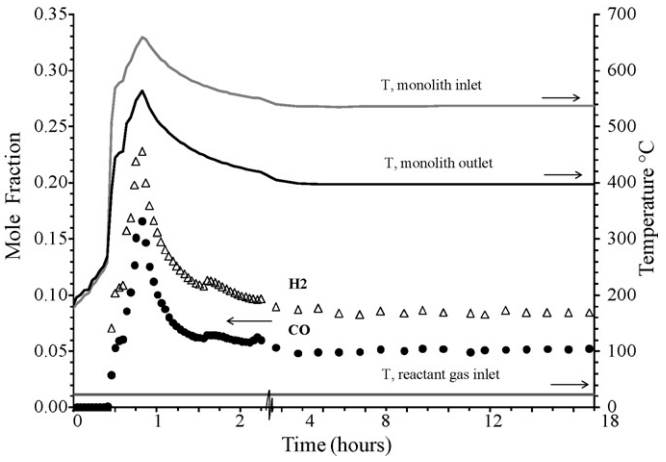

Fig. 11. 1.4:1 CH_4:CO_2 mixture sustained ATR for 17 h.

temperature. This ability to tune the H_2:CO ratio is beneficial because Fischer–Tropsch processes use H_2:CO mixtures with ratios ranging from 1 to 2 depending on the desired product. Gas mixtures with high H_2:CO ratios also have higher flame stability, due to the high reactivity of H_2, and can be used to enhance the reactivity of a landfill gas. Finally, the addition of an oxidant reduces carbon formation potential, as discussed and shown in Fig. 2, which allows the catalyst to maintain activity. These benefits are most fully realized if pure O_2 is used as the oxygen source, as opposed to air which will dilute the product gases.

3.4. Auto-thermal operation

Once there was a good understanding of the reactions occurring during auto-thermal reforming, the reactor was operated auto-thermally without heat input from an external heat source. A 1.4:1 CH_4:CO_2 mixture in 13.5% N_2 was heated to approximately 250 °C, above the catalytic ignition temperature of CH_4, at which point O_2 was introduced, for a resulting gas mixture of 41% CH_4, 29% CO_2, 11% N_2 and 19% O_2. The inlet and outlet monolith temperatures and product mole fractions were measured. As expected, the O_2 introduction resulted in a sharp increase in monolith temperature due to combustion and partial oxidation of CH_4, causing the inlet monolith temperature to increase to 581 °C while the exit temperature increased to 455 °C. The furnace temperature was then increased at a rate of approximately 7 °C min^{-1} until the monolith inlet temperature was 660 °C with an outlet temperature of 564 °C.

The outlet temperature of the monolith is lower than the inlet temperature in each case because the inlet temperature is measuring the heat produced from the exothermic combustion and partial oxidation reactions that occur rapidly at the front face of the monolith. The endothermic reforming reactions occur throughout the monolith, resulting in a lower monolith outlet temperature. As the furnace temperature is increased, the temperature gradient in the monolith decreases slightly, shown in Fig. 11, from ΔT = 125 °C at a monolith outlet temperature of 450 °C to ΔT = 95 °C at a monolith outlet temperature of 564 °C. This is likely a combination of higher rates of endothermic reforming reactions at elevated monolith temperatures, and higher rates of heat loss as the monolith temperature increases.

After the monolith was heated to an outlet temperature of 564 °C, the external heat source was turned off while the gas flow remained unchanged, and the reactor was allowed to cool. The reactor cooled until the monolith inlet temperature stabilized at 535 °C and the outlet temperature at 397 °C, while H_2 and CO were still being produced. The auto-thermal reaction sustained itself for 17 h, as shown in Fig. 11, until the O_2 was shut off, terminating the reaction. Throughout this time, the methane conversion and product compositions remained constant, and no visible darkening of the monolith was seen, suggesting that no noticeable coking or deactivation occurring during auto-thermal operation.

As shown in Fig. 11, the outlet temperature of the monolith was maintained at 400 °C, producing a H_2:CO ratio of approximately 1.7. This agrees well with Fig. 6 that shows that at a monolith outlet temperature of 400 °C, steam reforming, dry reforming, and water–gas shift are occurring, and agrees somewhat with Fig. 10 that shows that at 400 °C the H_2:CO ratio expected is 2.02. The CH_4 conversion was maintained at approximately 37% throughout auto-thermal operation. This corresponds with Table 4 that shows that at 400 °C, the expected CH_4 conversion is 33%.

4. Conclusions

A quartz flow-through reactor was designed and used to test the viability of a Rh/γAl_2O_3 monolithic catalyst for dry and auto-thermally reforming CH_4 and CO_2 gas mixtures. The Rh catalyst achieved equilibrium conversions of CH_4 and CO_2 to H_2 and CO for both 1:1 and 1.4:1 ratios of CH_4:CO_2 with and without O_2. No deactivation was seen while operating at 1:1 CH_4:CO_2 ratios, but some deactivation was seen after long-term (24 h) exposure to 1.4:1 ratios of CH_4:CO_2 without O_2. Deactivation was not seen after long-term exposure to 1.4:1 ratios of CH_4:CO_2 with O_2. Finally, the catalyst has shown that after coking it can be regenerated in air, evolving CO_2 and resulting in an activity recovery. More extensive testing focused on catalyst durability for 1:1 and 1.4:1 CH_4:CO_2 ratios with and without O_2 is in progress to better understand the conditions that lead to carbon formation.

Auto-thermal reforming was investigated by injecting pure O_2 into the CH_4:CO_2 mixtures and monitoring the evolved gases and monolith temperature. It was found that ATR results in combustion and partial oxidation of CH_4, providing heat and reactants (H_2O and CO_2) that lead to greater conversion of CH_4 to H_2 and CO compared to dry reforming alone. Using ATR, heat from methane combustion is produced in the channels of the reactor, reducing or eliminating the need for external process heat input. ATR is particularly valuable for gas mixtures with CH_4:CO_2 ratios higher than 1, which is common in landfill gas mixtures, because it ensures that the most valuable resource, CH_4, is converted to syngas. These benefits are most fully realized if pure O_2 is used as the oxygen source, as opposed to air which will dilute the product gases in N_2. Finally, ATR produces a range of H_2:CO ratios from 1.0 to 2.0 which can be tuned depending on the monolith temperature. This tuning ability is useful for downstream Fischer–Tropsch synthesis, for maximizing H_2 yields for a PEM fuel cell, or for using H_2 to produce a more reactive and reliable fuel source from landfill gas.

Sustained auto-thermal reforming, without external heat input, was demonstrated on a laboratory scale without catalyst deactivation or visible coking. In an industrial process, landfill gas could be reformed to H_2 and CO with only an initial energy input to initiate the methane combustion reaction, potentially reducing operating costs for LFG reforming.

Acknowledgements

The authors would like to thank the Catalysis and Combustion Laboratory at Columbia University, Columbia University Presidential Fellowship, and BASF Catalysts for supporting this research.

References

[1] L. Arsova, R. van Haaren, N. Goldstein, S.M. Kaufman, N.J. Themelis, Biocycle 49 (2008).

[2] N. Themelis, P. Ulloa, Renewable Energy 32 (2007) 1243–1257.
[3] Environmental Protection Agency. LMOP Landfill Database (2008) http://www.epa.gov/lmop/proj/index.htm#1.
[4] Waste Management, Inc. "Waste managment and Linde to develop the world's largest landfill gas to LNG facility.".(2008, April 4).
[5] D. Chen, R. Lodeng, A. Anundskas, O. Olsvik, A. Holmen, Chemical Engineering Science 56 (2001) 1371–1379.
[6] J.R. Ross, Catalysis Today 100 (2005) 151–158.
[7] J. Rostrup-Nielsen, Catlysis Today 18 (1993) 305–324.
[8] R.M. Heck, R.J. Farrauto, Catalytic Air Pollution Control, 3rd Edition., Wiley and Sons, Hoboken, NJ, 2009.
[9] Morley, C. GASEQ. Chemical Equilibria in perfect gases. (2005) http://www.gaseq.co.uk/.
[10] Outokumpu Research Oy. HSC Chemistry 5.1. (2002).
[11] A. Erdohelyi, J. Cserenyi, F. Solymosi, Journal of Catalysis 141 (1993) 287–299.
[12] Whitmore, Noah. Masters Thesis (2007). Columbia University.
[13] J. Munera, L.M. Cornaglia, D. Vargas Cesar, M. Schmal, E.A. Lombardo, Industrial and Engineering Chemistry Research 46 (2007) 7543–7549.
[14] J. Wei, E. Iglesia, Journal of Catalysis 224 (2004) 370–383.
[15] M. Maestri, D. Vlachos, A. Beretta, G. Groppi, E. Tronconi, Journal of Catalysis 259 (2008) 211–222.
[16] D.A. Hickman, L.D. Schmidt, Journal of Catalysis 138 (1992) 267–282.
[17] B. Michael, A. Donazzi, L. Schmidt, Journal of Catalysis 265 (2009) 117–129.
[18] S. Specchia, G. Negor, G. Saracco, V. Specchia, Applied Catalysis B 70 (2007) 525–531.
[19] J. Ruiz, F. Passos, J. Bueno, E. Souza-Aguiar, L. Mattos, F. Noronha, Applied Catalysis A 334 (2008) 259–267.
[20] M. Simeone, L. Salemme, C. Allouis, International Journal of Hydrogen Energy 33 (2008) 4798–4808.
[21] A. York, T. Xiao, M. Green, J. Claridge, Catalysis Reviews 49 (2007) 511–560.
[22] J. Grunwaldt, L. Basini, B. Clausen, Journal of Catalysis 200 (2001) 321–329.
[23] Y. Cui, H. Zhang, H. Xu, W. Li, Applied Catalysis A 318 (2007) 79–88.
[24] A. Nandini, K. Pant, S. Dhingra, Applied Catalysis A 308 (2006) 119–127.
[25] Z.E. Verykios, Applied Catalysis A 255 (2003) 101–111.
[26] S.-G. Wang, Y.-W. Li, J.-X. Lu, M.-Y. He, H. Jiao, Journal of Molecular Structure 673 (2004) 181–189.